ELSEVIER

Catalysis Today 48 (1999) 73–81

CATALYSIS TODAY

Xylose hydrogenation: kinetic and NMR studies of the reaction mechanisms

Jyri-Pekka Mikkola[a], Rainer Sjöholm[b], Tapio Salmi[a,*], Päivi Mäki-Arvela[a]

[a]*Åbo Akademi, Laboratory of Industrial Chemistry, Turku, Finland*
[b]*Åbo Akademi, Laboratory of Organic Chemistry, Turku, Finland*

Abstract

Hydrogenation of xylose over Raney nickel was studied in a batch reactor. A pseudo-homogeneous kinetic model was able to prognose the xylose and xylitol concentrations rather well. The obtained fit for the activation energies suggests that external diffusion limitations are absent in our experimental conditions. The sugar equilibria studies gave new information about the temperature dependence of the α–β-pyranose equilibria. It was found that the equilibria in D_2O follows an S-shaped curve, the equilibria being shifted towards the α-form at higher temperatures.

Keywords: Xylitol; Xylose; Monosaccharide; Raney nickel; Catalytic hydrogenation

1. Introduction

Liquid phase hydrogenation of aldoses on a porous metal catalyst is an important process in the synthesis of sugar alcohols. Mono- and disaccharides have long been used and developed as natural sweetening agents; glucose, sucrose and starch hydrolyzates being the most commonly utilized ones. Quite recently, the interest to substitute artificial sweeteners for these sugars has increased. Xylitol, a penta alcohol obtained by the hydrogenation of xylose, is an excellent choice of replacement. It is very soluble in water; it is optically inactive; its crystals resemble those of sugar; it is stable upon storage and it does not caramelize at elevated temperatures. The sweetening capacity of xylitol exceeds that of sugar by 20–25% and has no insulin requirements [1]. Xylitol is even used in pharmaceutical, cosmetic, synthetic resin and alimentary industries.

Xylitol is typically produced via batchwise, isothermal and isobaric hydrogenation processes, where aqueous xylose solutions are hydrogenated on a finely dispersed catalyst. Purification of xylose, usually carried out by means of ion-exchange, filtering and crystallization, is essential for the success of the consequent step, i.e. the hydrogenation of xylose to xylitol, since the most commonly used catalyst, Raney nickel, is easily poisoned and deactivated by the impurities in the starting material. In general, several known hydrogenation catalysts could in principle be used, such as noble metals (Pt, Pd, Ru) or nickel-based (especially Raney nickel) catalysts. Wisniak et al. [1,2] studied various metal catalysts in the hydrogenation of glucose, fructose and xylose. It was concluded that the activity of the catalytic metals decreases in the order Ru>Ni>Rh>Pd.

*Corresponding author.

0920-5861/99/$ – see front matter
PII: S0920-5861(98)00360-5

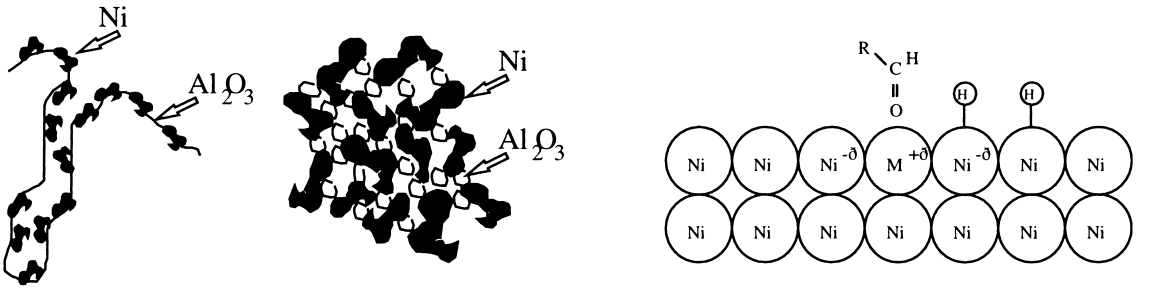

Fig. 1. Structure of Raney nickel catalyst and a plausible mechanism for the adsorption of monosaccharides on Ra-Ni.

The typical structure of Raney nickel as well as the component adsorption is illustrated in Fig. 1. The endeavor of the present work is to determine the kinetics of xylose hydrogenation on a commercial Raney nickel catalyst.

2. Experimental

The kinetic experiments were carried out in an automatic laboratory scale three-phase reactor system by Parr Instrument (Parr 4560, s.s.) with a total volume of 600 ml, equipped with a conventional propeller mixer, coupled to a Rushton turbine for effective gas dispersion. The liquid volume was always adjusted to approximately 300 ml. The temperature and stirrer controllers used were Parr 4843 (Watlow Controls Series 982). The minimum stirring rate necessary for the elimination of outer liquid–solid mass transfer resistances was found to be approx. 1500 rpm. In order to be sure that we operated within the chemically controlled regime, the speed of the stirrer was selected at 1750 rpm. To verify that the construction material of the reactor does not have any catalytic effect, a blank run without catalyst was carried out.

Before each experiment, the catalyst and the reactor vessel were preheated under hydrogen atmosphere to the desired temperature. Simultaneously, the xylose–solvent mixture was heated under nitrogen flow (15 min) in a preheater. Also, bubbling with hydrogen was tested, thus confirming that presaturation of the reactive mixture with nitrogen does not affect the reaction rate measurably in our experimental conditions. The liquid reactant–solvent mixture was fed into the reactor rapidly, after which the pressure was immediately adjusted to the experimental conditions. Simultaneously, the stirrer was switched on. This moment was considered as the initial starting time of the experiment. A Brooks Microprocessor Control & Read Out Unit (0152) was used for the pressure control. The reactor was operated in the pressure range 40–70 bar and at 80–140°C. The temperature and pressure profiles were recorded with a microcomputer. The concentration of xylose in the aqueous solvent was varied between 40 and 60 wt%. The water used was always deionized. Hydrogen had a purity of 99.999% (Oy AGA Ab).

A commercial Raney Ni catalyst, containing approximately 90 wt% Ni, was used. The amount of the catalyst was fixed at 5 wt% of the xylose weight. Malver Instruments' droplet and particle sizer 2600C (focal length 100 mm, beam length 2 mm) was used in the measurement of the particle size distribution. The average particle size was found to be 22.3 μm (50% of particles <22.3 μm, 90% <75.3 μm, 10% <5.1 μm). The particle size distribution is displayed in Fig. 2.

The reactor contents were analyzed off-line with a liquid chromatograph (HP 1100 LC Series) equipped with a HP 1047A RI-detector (operating at 40°C), degasser, double-channel binary pump and autosampler. A Biorad Aminex HPX-87C carbohydrate column with a precolumn was used in the analysis. The eluent used was HPLC-grade water with 0.002 M $Ca(NO_3)_2{\cdot}4H_2O$ for rejuvenation of the column. The column was heated to 60°C and the flowrate was adjusted to 0.4 ml/min. The analysis results were recorded with HP Chemstation software. Two analytical methods were developed to obtain as good as possible an accuracy of the calibration curves; i.e. one for the higher concentration domain and another for the lower one. The methods differed mainly in the injection volumes of the analysis sample. Generally,

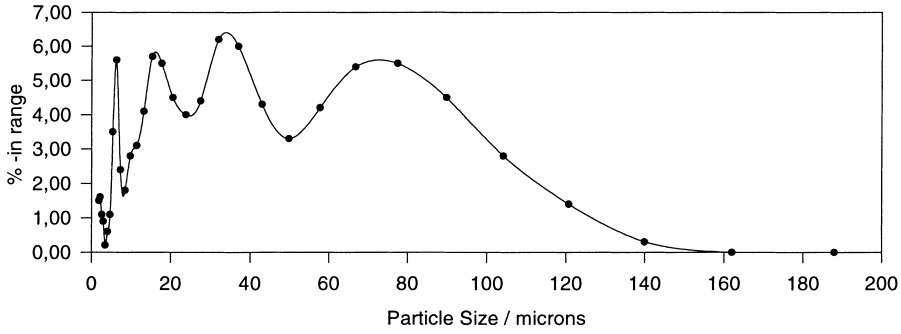

Fig. 2. Particle size distribution of Raney nickel.

the highest analytical error was typically within the range ±2 wt%. The samples to be analyzed were taken from the main bulk of the reacting mass by shortly cracking a sample valve, thus extracting less than 1 g of the liquid per sample. The removal of the catalyst was avoided by placing a filter in the sampling line. In the beginning of the experiment, the samples were withdrawn more frequently (every 2–5 min) than during the main course of the reaction (every 20 min). Since the amount of the samples extracted from the reactor was negligible, it was appropriate to consider the fluid volume in the reactor as constant. A schematic representation of the experimental apparatus is illustrated in Fig. 3.

^{1}H NMR spectra were recorded by a JEOL JNM-A500 FT NMR spectrometer operating at 500 MHz. The sample was prepared by dissolving 500 mg of xylose in 1 ml of D_2O. The sample was held for 1 h at each temperature before the measurement to allow for equilibration. Three measurements were performed at 10 min intervals at each temperature. In the quantitative analyzes of the equilibrium mixtures of α- and β-xylose the spectra were registered by the accumulation of four pulses using 65K data points which gave a digital resolution of 0.15 Hz. The pulse delay was 11 s which was found sufficient to avoid the effects of differences in the proton relaxation times. The signals of H-2 in the α-anomer and H-3 in the β-anomer were used for the integration of the signal intensities. The average of three measurements at each temperature was calculated. A ^{13}C NMR spectrum of the sample was also recorded at 80°C in a mode allowing quantitative analyses of the signal intensities, i.e. a pulse sequence eliminating NOE (nuclear overhauser effect) enhancement, and a pulse repetition time of 12 s. 32K

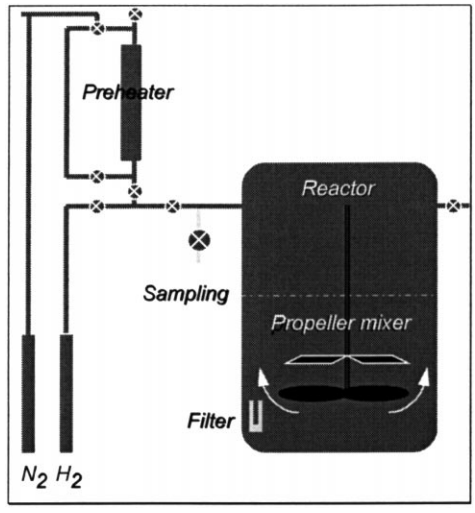

Fig. 3. The reactor system for xylose hydrogenation.

data points giving a digital resolution of 1 Hz were used.

3. Results and discussion

3.1. Sugar equilibria

The sugar equilibria are illustrated in Figs. 4 and 5. ^{1}H NMR spectroscopy in DMSO-d_6 showed that only α-xylopyranose could be observed in the solution immediately after the sample was dissolved. However, in D_2O at 30°C, the balance was shifted towards β-pyranose because of mutarotation. According to the literature [3], the furanose content at equilibrium in water is less than 1% at 30°C and is expected to increase at higher temperatures. The increase in the

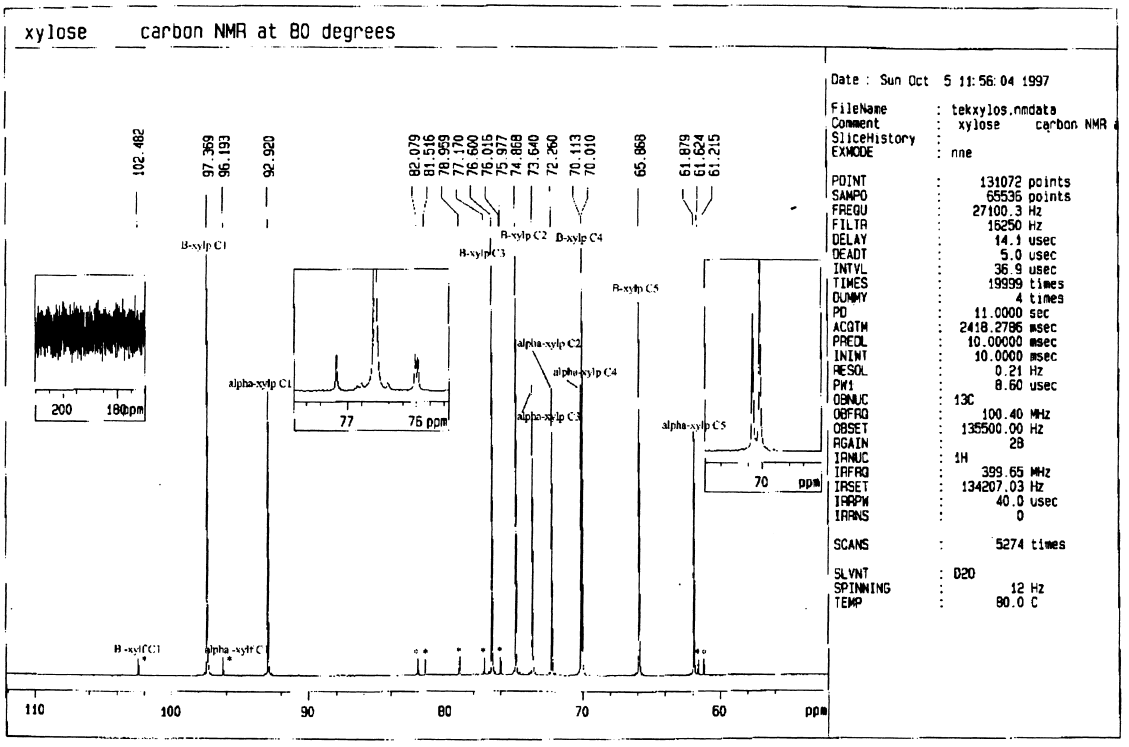

Fig. 4. Sample ^{13}C NMR spectra at 80°C.

relative amount of furanoses with increasing temperature is evident from the ^{13}C NMR spectrum taken at 80°C in D_2O (Fig. 4). The signals from the furanose units can be clearly seen in the spectrum. A quantitative measurement showed that in the pyranose/furanose mixture the furanoses comprised ca. 4.4 wt%. However, the carbon spectrum, with an insert with expansion in the *y*-direction of the carbonyl region, showed no signal which could be assigned to the carbon atom of an aldehyde group.

In Table 1, data on the relative distribution of the pyranose forms in D_2O are presented. Also, Fig. 6 demonstrates the temperature dependence of the pyranose equilibria. As can be seen from the figure, the pyranose equilibria are shifted towards α-pyranose with rising temperature.

3.2. *Xylose in D_2O (33.3 wt%)*

The anomer ratios are based on the measurement of the intensities of the signals of α H-2/β H-2 and α H-2/β H-3. PD=11 s (pulse delay) and PO=65K (data point). The measurement based on the α H-2 versus β H-3 signals gives the most reliable results.

Table 1
The pyranose equilibria

Temperature (°C)	Normalized anomer ratio in D_2O (%)			
	α-Anomer		β-Anomer	
	α H-2		β H-2	β H-3
20	35.6	35.7	64.4	64.3
20	35.5	35.5	64.5	64.5
20	36.2	35.0	63.8	65.0
40	36.0	35.5	64.0	64.5
40	35.7	35.5	64.3	64.5
40	36.1	35.5	63.9	64.5
60	37.3	36.9	62.7	63.1
60	36.8	36.7	63.2	63.3
60	37.0	37.1	63.0	62.9
80	39.1	39.1	60.9	60.9
80	39.7	38.4	60.3	61.6
80	39.3	38.9	60.7	61.1
100	40.0	39.2	60.0	60.8
100	41.6	40.4	58.4	59.6
100	40.2	39.8	59.8	60.2

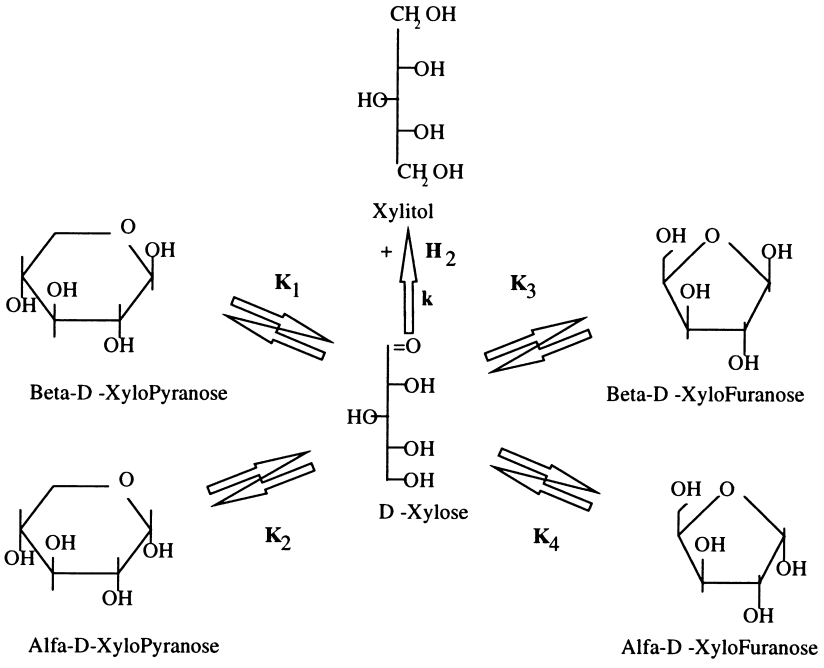

Fig. 5. The sugar equilibria.

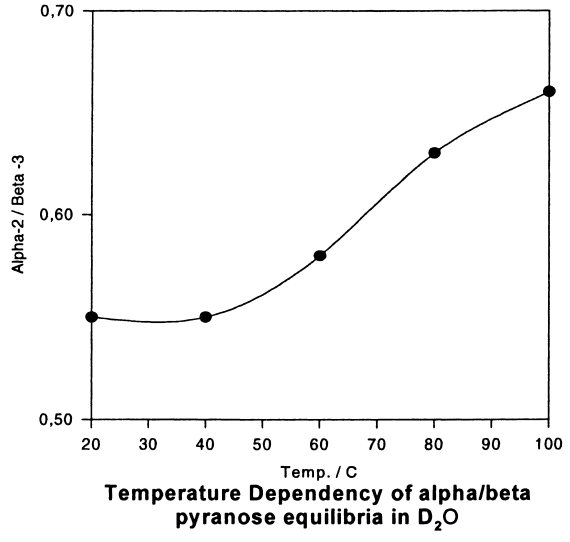

Fig. 6. Temperature dependency of the sugar equilibria.

3.3. Kinetic equations – model discrimination

Hydrogenation of the most common monosaccharides is extensively covered in the literature [4] by a multitude of authors. However, the literature on xylose hydrogenation is rather scarce. Wisniak et al. [1] studied the hydrogenation of xylose to xylitol and suggested that the overall reaction rate can be represented by pseudo-first order kinetics, i.e. $r=-kc$.

In this work, we try to develop a kinetic model for xylose hydrogenation based on plausible catalytic surface reaction mechanisms. One can usually obtain a relatively good fit for a number of rival kinetic models. The discrimination between the various models is usually not easy: a preferred approach is to relate the parameters to physical phenomena, i.e. rely on a mechanistic viewpoint.

3.4. Competitive pseudo-homogeneous adsorption model

In our approach the surface reaction between adsorbed xylose and hydrogen is assumed to be the rate-determining step (rds) and the remaining ones are presumed to proceed rapidly. Each of the involved species are assumed to occupy only one active site – a hypothesis, which can be heavily criticized. However, a more sophisticated approach is under consideration.

Diffusion resistances are included in the rate and adsorption coefficients in this simplified approach. Also, both hydrogen and xylose are assumed to compete on the same active center during the course of adsorption. Formation of by-products is strongly influenced by the pH of the reaction medium. Isomerization of sugars in aqueous media by alkali is a well-known scheme. In mildly acidic conditions, sugars are relatively stable. However, the leaching of Ni from the catalyst becomes a problem, if the pH of the reaction medium diminishes to very low values. Also, Ni-induced Cannizaro reaction in the presence of alkali, leading to xylonic acid formation, takes place. Our kinetic model, however, does not involve xylonic acid, since the experimental runs were all performed at mildly acidic–neutral conditions. The pH of the reaction medium varied somewhat randomly during the course of the hydrogenation. The general trend was, however, a drop of 1–2 units during a batch.

The HPLC analysis practically always displayed formation of xylulose, which after some time was consumed because of the hydrogenation to xylitol and arabinitol (lyxitol). The proposed reaction scheme is sketched in Fig. 7. The reaction steps of our model are shown in Fig. 8.

Provided that the volume of the liquid phase remains approximately constant (i.e. $V_L \approx$ constant), we arrive at the following set of mass balance equations, in which c_i denotes the concentration of substance i in the liquid phase

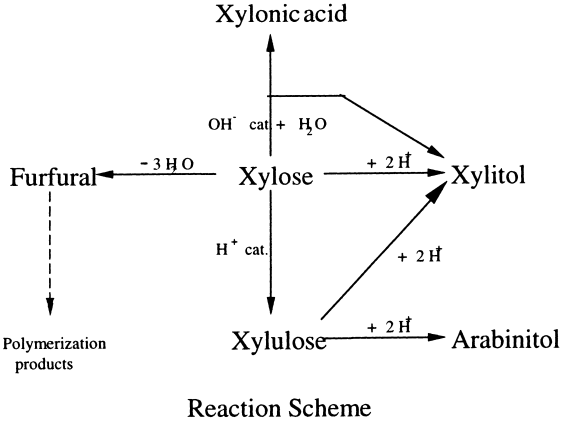

Fig. 7. Main and side reactions in xylose hydrogenation.

$$\frac{dc_i}{dt} = r_j \frac{m_{cat}}{V_L}. \quad (1)$$

The relation m_{cat}/V_L can be denoted as ρ_B, i.e. the catalyst bulk density, leading to

$$\frac{dc_i}{dt} = r_j \rho_B \quad (2)$$

in which $r_j = f(c_i)$. The coverage of the adsorbed components on the catalyst is denoted by Θ_j, and we obtain the following quasi-equilibria:

$$\Theta_j = \frac{c_{j\otimes}}{c_{\otimes tot}}, \quad (3)$$

$$\text{step 1:} \qquad K_s = \frac{\Theta_s}{c_s \Theta_{free}}, \quad \text{i.e.} \quad \Theta_s = K_s c_s \Theta_{free} \quad (4)$$

in which $c_{\otimes tot}$ denotes the total concentration of active sites. For dissociative adsorption of hydrogen on the catalyst surface the following expression is derived:

$$\text{step 2:} \qquad K_H = \frac{\Theta_H^2}{c_H \Theta_{free}^2}, \quad \text{i.e.} \quad \Theta_H = \sqrt{K_H}\sqrt{c_H}\Theta_{free}. \quad (5)$$

The xylulose formation is assumed to follow a first order rate law. The mechanistic principle of xylulose formation is presented in Fig. 9.

$$\text{step 3:} \qquad c_{xy} = K_{isom} c_s, \quad (6)$$

$$\text{step 4:} \qquad K_{xy} = \frac{\Theta_{xy}}{c_{xy}\Theta_{free}}, \quad \text{i.e.} \quad \Theta_{xy} = K_{xy} c_{xy} \Theta_{free}. \quad (7)$$

For the rate-determining steps, for xylose and xylulose hydrogenation we obtain

$$\text{step 5:} \qquad R_1 = k_{RDS,X1} \Theta_s \Theta_H^2, \quad (8)$$

$$\text{step 6:} \qquad R_2 = k_{RDS,X2} \Theta_{xy} \Theta_H^2. \quad (9)$$

Analogously, for the hydrogenation of xylulose to D-arabinitol we get

$$\text{step 8:} \qquad R_3 = k_{RDS,A} \Theta_{xy} \Theta_H^2. \quad (10)$$

For the adsorption–desorption quasi-equilibria for xylitol and arabinitol we have

$$\text{step 7:} \qquad K_x = \frac{\Theta_x}{c_x \Theta_{free}}, \quad \text{i.e.} \quad \theta_x = K_x c_x \theta_{free}, \quad (11)$$

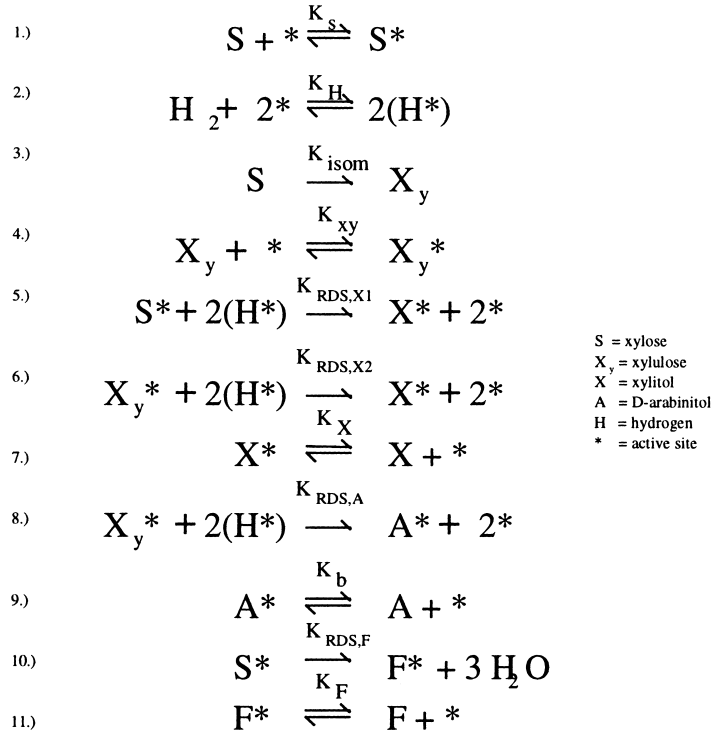

Fig. 8. Reaction steps.

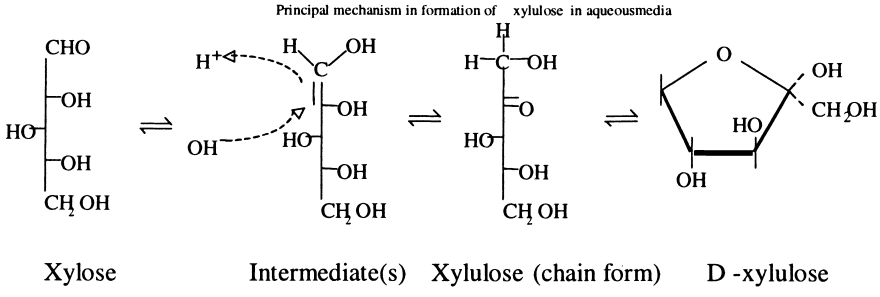

Fig. 9. Isomerization of xylose to xylulose.

$$\text{step 9}: \quad K_A = \frac{\Theta_A}{c_A \Theta_{free}}, \quad \text{i.e.} \quad \theta_A = K_A c_A \theta_{free}. \tag{12}$$

For the furfural formation, which is promoted by high reaction temperatures we get

$$\text{step 10}: \quad R_4 = k_{RDS,F}\Theta_s \tag{13}$$

and analogously, for the desorption of furfural to the main bulk of the reaction solvent

$$\text{step 11}: \quad K_F = \frac{\Theta_F}{c_F \Theta_{free}}, \quad \text{i.e.} \quad \theta_F = K_F c_F \Theta_{free}. \tag{14}$$

The total site-balance is defined as follows:

$$\theta_s + \theta_x + \theta_F + \theta_H + \theta_A + \theta_{free} = 1. \tag{15}$$

The kinetic expressions for the rate-determining steps are presented in the sequel.

For the surface reaction for hydrogenation of xylose we obtain

$$R_1 = \frac{c_s c_H}{\left(a_{11} + a_{12}c_s + a_{13}c_x + a_{14}c_A + a_{15}c_F + a_{16}\sqrt{c_H}\right)^3}, \quad (16)$$

where $a_{11}=(1/(k_{RDS,X1}K_sK_H)^{1/3})$, $a_{12}=(K_s+K_{xy}-K_{isom})a_{11}$, $a_{13}=K_xa_{11}$, $a_{14}=K_Aa_{11}$, $a_{15}=K_xa_{11}$, and $a_{16}=\sqrt{K_H}a_{11}$.

In the case of xylulose hydrogenation into xylitol we arrive at the following expression:

$$R_2 = \frac{c_{xy} c_H}{\left(a_{21} + a_{22}c_s + a_{23}c_x + a_{24}c_A + a_{25}c_F + a_{26}\sqrt{c_H}\right)^3}, \quad (17)$$

where $a_{21}=(1/(k_{RDS,X2}K_{xy}K_H)^{1/3})$, $a_{22}=(K_s+K_{xy}-K_{isom})a_{21}$, $a_{23}=K_xa_{21}$, $a_{24}=K_Aa_{21}$, $a_{25}=K_Fa_{21}$, and $a_{26}=\sqrt{K_H}a_{21}$.

Analogously, for the xylulose hydrogenation into arabinitol, we get the following set of rate equations:

$$R_A = \frac{c_{xy} c_H}{\left(b_1 + b_2c_s + b_3c_x + b_4c_A + b_5c_F + b_6\sqrt{c_H}\right)^3}, \quad (18)$$

where $b_1=(1/(k_{RDS,A}K_{xy}K_H)^{1/3})$, $b_2=(K_s+K_{xy}K_{isom})-b_1$, $b_3=K_xb_1$, $b_4=K_Ab_1$, $b_5=K_5b_1$, and $b_6=\sqrt{K_H}b_1$.

Finally, for the formation of furfural

$$R_F = \frac{c_s}{\left(g_1 + g_2c_s + g_3c_x + g_4c_A + g_5c_F + g_6\sqrt{c_H}\right)}, \quad (19)$$

where $g_1=1/(k_{RDS,F}K_s)$, $g_2=(K_s+K_{xy}K_{isom})g_1$, $g_3=K_xg_1$, $g_4=K_Ag_1$, $g_5=K_xg_1$ and $g_6=\sqrt{K_H}g_1$.

Since furfural, de facto, polymerizes in the actual reaction conditions and thus escapes beyond the analysis, we implemented a dummy second order reaction for the formation of unidentified polymerization products, *P*. Thus, furfural, that is formed, is almost immediately consumed by oligomerization.

The parameter fitting was performed with the Modest software [5] using a combined Simplex–Levenberg–Marquardt method. The model agreement to the experimental data was typically better than 95%. Although the amount of parameters to be fitted was rather large (14%), the correlation matrix showed very low correlation between the parameters. Typical experimental curves and model fits are presented in Fig. 10. As can be seen from the figure, the oveit model describes rather well the kinetics of the main components. At present, the fit of the side-reactions is not yet satisfactory.

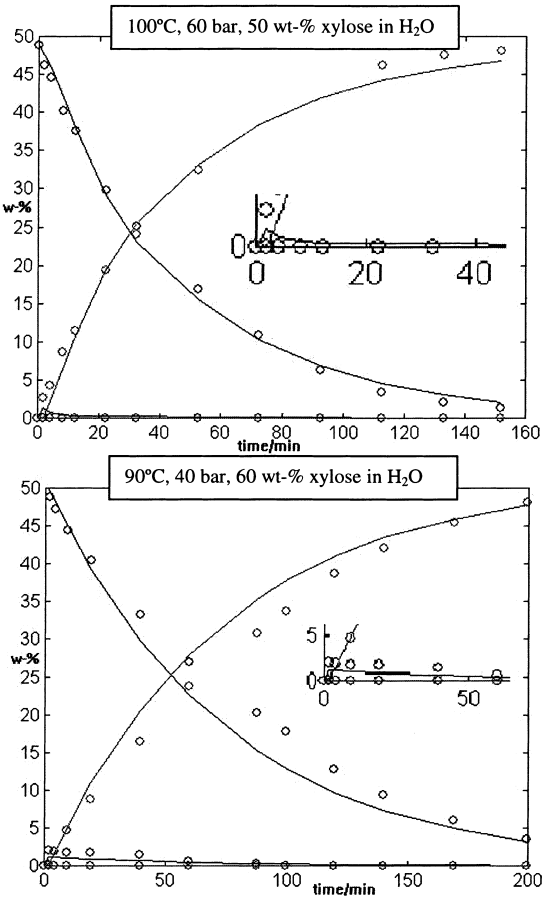

Fig. 10. Two sample model fits.

4. Conclusions

Our simple kinetic model is able to predict the xylose and xylitol concentrations with better than 95% accuracy. The obtained activation energies suggest that the external diffusion is not a limiting factor in the process (magnitude of 10^5 J/mol). The model currently approximates the hydrogen solubility as that of its solubility in water. Measurements are needed for more reliable prognosis of hydrogen solubility in this

multi-component mixture and pH data collected during the course of reaction is not yet taken into account. As stated earlier, the formation of by-products is affected by the pH of the reaction medium. The variations in pH are probably mainly due to two separate factors: auto-proteolysis of water on catalyst and remains of NaOH in the catalyst pores.

Acknowledgements

The scientific consultance of Mr. Heikki Heikkilä, Mr. Matti Tylli and Mrs. Riitta Hinkkanen (Xyrofin Oy) is gratefully acknowledged. The project was financially supported by the Technology Development centre (TEKES) and Xyrofin Oy.

References

[1] J. Wisniak et al., Ind. Eng. Chem. Prod. Res. Dev. 13(1) (1974) 75.
[2] J. Wisniak et al., Ind. Eng. Chem. Prod. Res. Dev. 13(4) (1974) 232.
[3] P. Collins, R. Ferrier, Monosaccharides, Wiley, Chichester, 1995.
[4] R. Albert, A. Strätz, G. Vollheim, Chem. Ing. Tech. 52(7) (1980) 582.
[5] H. Haario, MODEST User's Manual, Profmath Oy, Helsinki, 1994.